Magnetometer Modeling and Validation for Tracking Metallic Targets

Niklas Wahlström, *Student Member, IEEE*, and Fredrik Gustafsson, *Fellow, IEEE*

***Abstract*—With the electromagnetic theory as a basis, we present a sensor model for three-axis magnetometers suitable for localization and tracking as required in intelligent transportation systems and security applications. The model depends on a physical magnetic dipole model of the target and its relative position to the sensor. Both point target and extended target models are provided as well as a heading angle dependent model. The suitability of magnetometers for tracking is analyzed in terms of local observability and the Cramér–Rao lower bound as a function of the sensor positions in a two sensor scenario. The models are validated with real field test data taken from various road vehicles which indicate excellent localization as well as identification of the magnetic target model suitable for target classification. These sensor models can be combined with a standard motion model and a standard nonlinear filter to track metallic objects in a magnetometer network.**

***Index Terms*—Magnetometers, tracking, magnetic dipole, observability.**

I. Introduction

TRACKING and classification of targets are primary concerns in automated surveillance and security systems. The tracking and classification information can be used for statistical purposes, i.e., counting number of targets of a specific type and registration of their velocities and directions of arrival. In this work we will focus on metallic targets.

One way of sensing metallic objects is by making use of their magnetic properties. We know that metallic objects induce a magnetic field partly due to its permanently magnetized ferromagnetic content and partly due to the deflection of the earth magnetic field [1]. This induced magnetic field can be measured with distributed passive magnetometers [2], [3].

For moving metallic vehicles, the magnetometer measurements will vary in time, which results in a time dependent signal. Like in other common tracking application based on radar, time difference of arrival and received signal strength, this signal depends on the position, speed, orientation and target specific parameters. The difference between the applications is summarized in the sensor model that relates the quantities to the observations. The same motion models and filters can be used in all these application. However, we do not focus on suggesting particular motion models and filters since these choices are standard in literature. Instead, we focus on the application specific fundamental questions of observability and geometry for the sensor model.

The simplest far-field model for the metallic vehicle is to approximate it as a moving magnetic dipole, which is parametrized with the magnetic dipole moment $\mathbf{m}$ that can be interpreted as the magnetic signature of the vehicle. This dipole model has previously been used for classification and target tracking of ground targets in [4]–[16]. In a near-field scenario the signal structure is much more complex where nonparametric methods have been shown to be successful. In [17], [18] an extensive investigation is presented, where the measured signal itself has been interpreted as the magnetic signature, which can be used for classification and re-identification of the vehicle at a different location. Furthermore, several studies have been done exploring the use of underwater magnetometers for tracking of vessels [19]–[21], where [21] has used the dipole model not only for localizing the vessel, but also for estimating the positions of the sensors. In [20] a Bayesian match-field approach has been used, which takes the attenuation of the seawater into consideration.

As in [4]–[16], [21], this work will be based on the dipole model. Similar to [4]–[7], [9]–[12] the theory will be applied on experimental data. However, we will generalize some important assumptions that previously have been made:

- Prior work [5]–[16] is constrained to a single dipole point target model, which does not included the geometrical extend of the target. We suggest a model with multiple dipoles. This model was suggested by Wynn [4] without being illustrated on simulated or real data, which will be provided in this work.
- Work in [4]–[10] is based on a linear motion assumptions, which simplifies the modeling of the dipole moment $\mathbf{m}$. However, for other motions where the target orientation changes over time, the dependency on $\mathbf{m}$ will be more complicated. One way of solving this is to marginalize the dipole moment as in [12]–[14]. However, this work will explicitly describe the $\mathbf{m}$ as a function of the target orientation.

We will derive a general sensor model for extended magnetic targets with target orientation dependent dipole moments observed in an arbitrary magnetometer network, where we validate the models using statistical tools for a variety of vehicles.

Furthermore, in [16] the problem with lack of observability for a one-sensor scenario has been addressed. Our work will more precisely describe this unobservable manifold. Also the optimal sensor deployment is analyzed in terms of local observ-

Manuscript received December 10, 2012; revised April 09, 2013; accepted July 05, 2013. Date of publication July 24, 2013; date of current version January 13, 2014. The associate editor coordinating the review of this manuscript and approving it for publication was Prof. Sofiene Affes. This work is supported by the Swedish Foundation for Strategic Research under the project Cooperative Localization. A preliminary version of this paper was presented at the Thirteenth International Conference on Information Fusion (FUSION), Edinburgh, U.K., 2010.

The authors are with the Department of Electrical Engineering, Division of Automatic Control, Linköping University, Linköping, SE 581-83, Sweden (e-mail: nikwa@isy.liu.se; fredrik@isy.liu.se)

Color versions of one or more of the figures in this paper are available online at http://ieeexplore.ieee.org.

Digital Object Identifier 10.1109/TSP.2013.2274639

ability and the *Cramér Rao Lower Bound* (CRLB) as a function of the sensor positions.

The paper outline is as follows: Section II describes the sensor model and its extensions. In Section III a constant velocity tracking model is presented and compared with other models from the literature based on the same assumption. In Section IV observability and sensor deployment is discussed and in Section V the estimation methods are summarized. A validation of the sensor model based on experimental data is provided in Section VI. The paper closes with conclusions and proposals for future work.

II. Theoretical Sensor Model

In the statistical signal processing framework, a sensor model of a time-invariant system is given by

$$\mathbf{y}_k = \mathbf{h}(\mathbf{x}_k) + \mathbf{e}_k, \tag{1}$$

where $\mathbf{y}_k$ is the measurement, $\mathbf{x}_k$ is the state of the system and $\mathbf{e}_k$ is measurement noise, all at time instant kT_s, T_s being the sample period. This section will present and discuss different sensor models suitable for target tracking of magnetic objects.

A. Single Sensor Point Target Model

Any magnetic target will induce a magnetic field, which can be measured by a magnetometer. By approximating the target as a magnetic dipole [1], this field can be modeled as a magnetic dipole field. An expression of this field can be derived from Maxwell's equations [22] (for a derivation see for example [1]) and gives the following nonlinear model

$$\mathbf{h}(\mathbf{x}_k) = \mathbf{B}_0 + \frac{\mu_0}{4\pi}\frac{3(\mathbf{r}_k \cdot \mathbf{m}_k)\mathbf{r}_k - \|\mathbf{r}_k\|^2\mathbf{m}_k}{\|\mathbf{r}_k\|^5} \tag{2a}$$

$$= \mathbf{B}_0 + \mathrm{J}^{\mathbf{m}}(\mathbf{r}_k)\mathbf{m}_k, \tag{2b}$$

with

$$\mathrm{J}^{\mathbf{m}}(\mathbf{r}_k) = \frac{\mu_0}{4\pi\|\mathbf{r}_k\|^5}\left(3\mathbf{r}_k\mathbf{r}_k^{\mathsf{T}} - \|\mathbf{r}_k\|^2\mathrm{I}_3\right), \tag{2c}$$

where $\mathbf{B}_0$ is a bias, $\mathbf{r}_k$ is the position of the target relative to the sensor, $\mathbf{m}_k$ is the magnetic dipole moment of the target and $\mathbf{e}_k \sim \mathcal{N}(\mathbf{0}, \mathrm{R})$ white Gaussian noise. The total sensor model is then given by

$$\mathbf{y}_k = \mathbf{h}(\mathbf{x}_k) + \mathbf{e}_k \tag{2d}$$

$$\text{with} \quad \mathbf{x}_k = [\,\mathbf{B}_0^{\mathsf{T}} \quad \mathbf{r}_k^{\mathsf{T}} \quad \mathbf{m}_k^{\mathsf{T}}\,]^{\mathsf{T}}, \tag{2e}$$

The dipole model is an approximation of the induced magnetic field by considering the target to be a point source. This approximation is valid if the target is far from the sensor compared to its size, see Section II.C.

The bias $\mathbf{B}_0$ will in theory be constant and equal to the earth magnetic field. However, in practice it also includes the magnetic distortion induced by other metallic objects in the environment, which we assume to be constant. Furthermore, the bias $\mathbf{B}_0$ also includes a magnetic sensor bias, which slightly depends on temperature. This temperature may vary over time due to changing weather condition and amount of daylight exposed to the sensor [17]. However, this drift is slowly varying and is assumed to be constant during the time it takes for a vehicle to pass the sensor.

B. Multiple Sensor Model

The sensor model (2) can easily be extended to handle multiple sensors by introducing

$$\mathbf{h}_j(\mathbf{x}_k) = \mathbf{B}_{0,j} + \mathrm{J}^{\mathbf{m}}(\mathbf{r}_k - \boldsymbol{\theta}_j)\mathbf{m}_k \tag{3a}$$

where $\boldsymbol{\theta}_j$ and $\mathbf{B}_{0,j}$ are the position and the bias of the jth sensor respectively.

The total sensor model is then given by

$$\mathbf{y}_{j,k} = \mathbf{h}_j(\mathbf{x}_k) + \mathbf{e}_{j,k} \tag{3b}$$

$$\text{with} \quad \mathbf{x}_k = [\,\mathbf{B}_{0,1:J}^{\mathsf{T}} \quad \mathbf{r}_k^{\mathsf{T}} \quad \mathbf{m}_k^{\mathsf{T}}\,]^{\mathsf{T}}, \tag{3c}$$

where $\mathbf{e}_{j,k}$ is the measurement noise of the jth sensor.

C. Extended Target Model

The dipole model (2b) approximates the target with a single magnetic dipole and can as such be seen as a point target model. However, this is a fairly rough approximation since vehicles do have a geometrical extension. By parameterizing the extended target with multiple dipoles, a more accurate model can be obtained. By that we get an extended target model. Consider each dipole to be placed at $\Delta\mathbf{r}_k^i$, relative to the center of the target $\mathbf{r}_k$ and having the dipole vector $\mathbf{m}_k^i$. Then the point target model (2b) can be extended as

$$\mathbf{h}(\mathbf{x}_k) = \mathbf{B}_0 + \sum_{i=1}^{d} \mathrm{J}^{\mathbf{m}}\left(\mathbf{r}_k + \Delta\mathbf{r}_k^i\right)\mathbf{m}_k^i \tag{4}$$

where d is the number of dipoles. The extended target model in (4) reduces to a single target model (2b) if the relative positions $\Delta\mathbf{r}_k^i$ are much smaller than $\mathbf{r}_k$. The influence of the target extension can be analyzed by applying a Taylor series expansion of $\mathrm{J}^{\mathbf{m}}(\mathbf{r}_k)$ in (2c) around $\mathbf{r}_k$. By truncating the Taylor series after the second term, we reach the approximation

$$\mathbf{h}(\mathbf{x}_k) \approx \mathbf{B}_0 + \sum_{i=1}^{d}\left(\mathrm{J}^{\mathbf{m}}(\mathbf{r}_k) + \underbrace{\boldsymbol{\nabla}_{\mathbf{r}}(\mathrm{J}^{\mathbf{m}}(\mathbf{r}_k))\Delta\mathbf{r}_k^i}_{\triangleq \mathrm{J}^{\mathbf{r}}(\mathbf{r}_k, \Delta\mathbf{r}_k^i)}\right)\mathbf{m}_k^i$$

$$= \mathbf{B}_0 + \mathrm{J}^{\mathbf{m}}(\mathbf{r}_k) \times \sum_{i=1}^{d}\left(\mathrm{I}_3 + (\mathrm{J}^{\mathbf{m}}(\mathbf{r}_k))^{-1}\,\mathrm{J}^{\mathbf{r}}\left(\mathbf{r}_k, \Delta\mathbf{r}_k^i\right)\right)\mathbf{m}_k^i, \tag{5}$$

where we have defined

$$\{\boldsymbol{\nabla}_{\mathbf{x}}\mathbf{f}(\mathbf{x})\}_{i_1,\ldots,i_{n+1}} = \frac{\partial}{\partial x_{i_{n+1}}} f_{i_1,\ldots,i_n}(\mathbf{x}) \tag{6}$$

and $\mathrm{J}^{\mathbf{r}}(\cdot,\cdot)$ is given by (30b). Further, it can be shown that

$$\|\,(\mathrm{J}^{\mathbf{m}}(\mathbf{r}_k))^{-1}\,\mathrm{J}^{\mathbf{r}}\left(\mathbf{r}_k, \Delta\mathbf{r}_k^i\right)\|_2 \leq \frac{8}{7}\frac{\|\Delta\mathbf{r}_k^i\|_2}{\|\mathbf{r}_k\|_2} \tag{7}$$

and with $\|\Delta\mathbf{r}_k^i\|_2 \ll \|\mathbf{r}_k\|_2$ we arrive at the point target model

$$\mathbf{h}(\mathbf{x}_k) \approx \mathrm{J}^{\mathbf{m}}(\mathbf{r}_k)\sum_{i=1}^{d}\mathbf{m}_k^i = \mathrm{J}^{\mathbf{m}}(\mathbf{r}_k)\mathbf{m}_k, \tag{8}$$

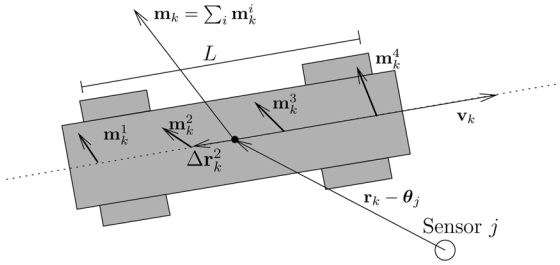

Fig. 1. The vehicle parametrized with $d = 4$ dipoles aligned in a row in the direction of the vehicle course $\mathbf{v}_k$. All dipoles are equally distanced with the interval $L/(d-1)$, i.e., a total length of L.

where the dipole moment $\mathbf{m}_k$ in point target model is related to the dipole moments $\mathbf{m}_k^i$ in the extended target models as

$$\mathbf{m}_k = \sum_{i=1}^{d} \mathbf{m}_k^i. \tag{9}$$

Thus, the point target model is valid if the distance between the target and the sensor is much larger than the characteristic length of the target, which has also been stated in [1]. However, if this is not the case an extended target model might be considered.

D. Uniformly Linear Array of Dipoles

In this work, a row of dipoles will be analyzed. Since a vehicle normally has its largest geometrical extension in the same direction as its course, a row of equidistantly distributed dipoles along the velocity vector $\mathbf{v}_k$ will be considered (see Fig. 1). The velocity vector $\mathbf{v}_k$ will later be included in the dynamic description in Section III. Furthermore, the size of the object is unknown, thus the distance between the first and the last dipole L has to be regarded as a parameter. By combining this with the multiple sensor model (3) we get

$$\mathbf{h}_j^d(\mathbf{x}_k) = \mathbf{B}_{0,j} + \sum_{i=1}^{d} \mathrm{J}^{\mathrm{m}}\left(\mathbf{r}_k - \boldsymbol{\theta}_j + \Delta\mathbf{r}_k^i\right)\mathbf{m}_k^i \tag{10a}$$

with

$$\Delta\mathbf{r}_k^i = \left(i - \frac{d+1}{2}\right)\frac{L}{d-1}\frac{\mathbf{v}_k}{\|\mathbf{v}_k\|}. \tag{10b}$$

The total sensor model is given by

$$\mathbf{y}_{j,k} = \mathbf{h}_j^d(\mathbf{x}_k) + \mathbf{e}_{j,k} \tag{10c}$$

$$\text{with} \quad \mathbf{x}_k = \left[\,(\mathbf{B}_{0,1:J})^{\mathsf{T}} \quad \mathbf{r}_k^{\mathsf{T}} \quad \mathbf{v}_k^{\mathsf{T}} \quad (\mathbf{m}_k^{1:d})^{\mathsf{T}} \quad L\,\right]^{\mathsf{T}}. \tag{10d}$$

Note that if either the length is $L = 0$ or the number of dipoles is $d = 1$, the model (10) will be equivalent with the point target model presented in (2).

E. Target Orientation Dependent Model

The magnetic dipole moment $\mathbf{m}_k$ will also depend on the orientation of the vehicle. To describe this dependency, the source of the magnetization has to be decomposed into one hard iron contribution and one soft iron contribution as done in [5], [13].

We know that metallic objects induce a magnetic field partly due to the ferromagnetic content (hard iron) and partly due to the deflection of the earth magnetic field (soft iron). The magnetization due to the hard iron can be represented with a magnetic dipole moment $\mathbf{m}_0$, which is independent of the external magnetic field and will thus always be constant in the reference frame of the vehicle. Since the sensors have the same reference frame as the world, which is not the same as the one of the vehicle, a transformation between these two reference frames has to be found. Generally, the heading Ψ, banking ϕ and inclination θ angles are used to define the relative orientation of a vehicle with respect to world coordinates. Here, the world coordinates are aligned with the magnetic north, see Fig. 2. In this work, no banking and inclination are considered since we assume that the road is flat, i.e., it does neither bank nor incline. Furthermore, any slip is neglected. Consequently, the heading Ψ_k uniquely determines the orientation of the vehicle with respect to the sensors and is defined as

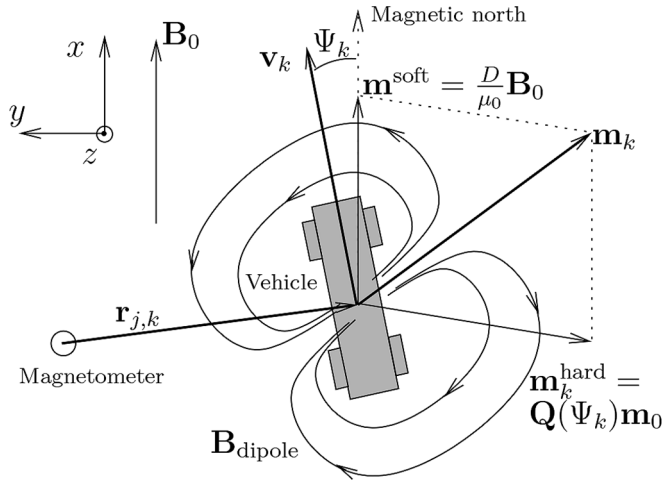

Fig. 2. A stationary magnetometer measures the earth magnetic field $\mathbf{B}_0$ together with a magnetic dipole field $\mathbf{B}_{\text{dipole}}$. The magnetic dipole field is induced by a moving vehicle at position $\mathbf{r}_{j,k}$ with velocity $\mathbf{v}_0$ and magnetic dipole moment $\mathbf{m}_k = \mathrm{Q}(\Psi_k)\mathbf{m}_0 + \frac{D}{\mu_0}\mathbf{B}_0$. The heading angle Ψ_k is defined by the velocity direction.

$$\Psi_k = \arctan2\left(v_k^{\mathrm{y}},\, v_k^{\mathrm{x}}\right), \tag{11}$$

with $\arctan2$ being the four quadrant arc-tangent. Now, with the rotation matrix

$$\mathrm{Q}(\Psi_k) = \begin{bmatrix} \cos\Psi_k & -\sin\Psi_k & 0 \\ \sin\Psi_k & \cos\Psi_k & 0 \\ 0 & 0 & 1 \end{bmatrix}, \tag{12}$$

the hard iron contribution of magnetic dipole moment can be described as

$$\mathbf{m}_k^{\text{hard}} = \mathrm{Q}(\Psi_k)\mathbf{m}_0. \tag{13}$$

On the other hand, the magnetization due to the soft iron is more complicated. For an isotropic medium (a spherical shell for example), the induced magnetic dipole moment $\mathbf{m}_{\text{soft}}$ is parallel to the earth magnetic field $\mathbf{B}_0$

$$\mathbf{m}^{\text{soft}} = \frac{D}{\mu_0}\mathbf{B}_0, \tag{14}$$

with D being a target characteristic scalar constant.

However, in general the moment induction is a non-isotropic process and its description requires a symmetric 3×3-matrix

P, which is known as the polarizability tensor [1]. In world coordinates this tensor reads $\mathrm{Q}(\Psi_k)\mathrm{P}\mathrm{Q}^{\mathsf{T}}(\Psi_k)$ and we have

$$\mathbf{m}_k^{\text{soft}} = \frac{1}{\mu_0}\mathrm{Q}(\Psi_k)\mathrm{P}\mathrm{Q}^{\mathsf{T}}(\Psi_k)\mathbf{B}_0.$$

Since a symmetric 3×3-matrix has 6 unknowns, this would heavily enlarge our state space dimension (and presumably lead to unobservability). Therefore, in this work we assume that magnetic dipole moment is parallel to the earth magnetic field. Thus we assume that the vehicles are isotropic, which might be a rough but workable assumption.

Since magnetization is additive, the total magnetic dipole moment can be modeled as

$$\mathbf{m}_k = \mathrm{Q}(\Psi_k)\mathbf{m}_0 + \frac{D}{\mu_0}\mathbf{B}_0. \tag{15}$$

In Fig. 2 a graphical representation of the model is presented.

We have now decomposed the magnetic dipole moment into two components, one representing the hard iron and one representing the soft iron. The corresponding model parameters D and $\mathbf{m}_0$ will represent the real magnetic signature of the target and will thus be constant even in a target maneuvering scenario.

F. General Sensor Model

The orientation dependent sensor model can now be combined with the extended target model (10) which gives

$$\mathbf{h}_j^d(\mathbf{x}_k) = \mathbf{B}_{0,j} + \sum_{i=1}^{d} \mathrm{J}^{\mathbf{m}}\left(\mathbf{r}_k + \Delta\mathbf{r}_k^i - \boldsymbol{\theta}_j\right)\mathbf{m}_k^i \tag{16a}$$

with

$$\mathbf{m}_k^i = \mathrm{Q}(\Psi_k)\mathbf{m}_0^i + \frac{D^i}{\mu_0}\mathbf{B}_0, \tag{16b}$$

$$\mathbf{B}_0 = \frac{1}{J}\sum_{j=1}^{J}\mathbf{B}_{0,j}, \tag{16c}$$

$$\Psi_k = \operatorname{arctan2}\left(v_k^{\mathsf{y}}, v_k^{\mathsf{x}}\right), \tag{16d}$$

$$\Delta\mathbf{r}_k^i = \left(i - \frac{d+1}{2}\right)\frac{L}{d-1}\frac{\mathbf{v}_k}{\|\mathbf{v}_k\|}. \tag{16e}$$

Here, the mean of all sensor biases $\mathbf{B}_{0,j}$ has been taken as an estimate of the earth magnetic field, which is needed for describing the orientation of the soft iron contribution (14). The total sensor model is then given by

$$\begin{aligned}\mathbf{y}_{j,k} &= \mathbf{h}_j^d(\mathbf{x}_k) + \mathbf{e}_{j,k}\\ \text{with}\quad \mathbf{x}_k &= \left[\,(\mathbf{B}_{0,1:J})^{\mathsf{T}} \quad \mathbf{r}_k^{\mathsf{T}} \quad \mathbf{v}_k^{\mathsf{T}} \quad (\mathbf{m}_0^{1:d})^{\mathsf{T}} \quad (D^{1:d})^{\mathsf{T}} \quad L\,\right]^{\mathsf{T}}\end{aligned} \tag{16f}$$

Note that if the heading Ψ_k is constant the magnetic dipole moment $\mathbf{m}_k^i$ will also be constant. Consequently, the parameters for the hard $\mathbf{m}_0^i$ and the soft iron D^i are not identifiable. Therefore, in such a scenario a parametrization of the dipole moment directly is more attractive solution, which will be used in the next section.

III. Constant Velocity Tracking Model

The models presented in the previous section are not constrained to any type of motion. However, in this work special interest will be given to the scenario when vehicles pass the sensor with constant velocity, i.e., a straight line motion with constant speed. This prior knowledge enables us to formulate a static sensor model.

A. Sensor Model for Constant Velocity

By assuming constant velocity $\mathbf{v}_k$

$$\begin{aligned}\mathbf{r}_{k+1} &= \mathbf{r}_k + T_s\mathbf{v}_k,\\ \mathbf{v}_{k+1} &= \mathbf{v}_k,\end{aligned} \tag{17}$$

the heading Ψ_k will also be constant as well as the magnetic dipole moment $\mathbf{m}_k$ according to (15). We could also consider another parametrization of the target motion. However, if that motion model implies a time-varying heading Ψ_k, the magnetic dipole moment will no longer be constant and the target orientation dependent dipole model (15) has to be considered.

We can now define a static sensor model

$$\begin{aligned}\mathbf{y}_k &= \mathbf{h}_k(\mathbf{x}) + \mathbf{e}_k\\ &= \mathbf{B}_0 + \frac{\mu_0}{4\pi}\frac{3(\mathbf{r}_k\cdot\mathbf{m})\mathbf{r}_k - \|\mathbf{r}_k\|^2\mathbf{m}}{\|\mathbf{r}_k\|^5} + \mathbf{e}_k,\\ &\quad \text{where}\quad \mathbf{r}_k = \mathbf{r}_0 + kT_s\mathbf{v}_0.\end{aligned} \tag{18}$$

Here, the substitution

$$\begin{aligned}\mathbf{r}_k &= \mathbf{r}_0 + kT_s\mathbf{v}_0\\ \mathbf{m}_k &= \mathbf{m}\end{aligned} \tag{19}$$

has been used in (2). Thus, now we have the parameter vector

$$\mathbf{x} = \left[\,\mathbf{B}_0^{\mathsf{T}} \quad \mathbf{r}_0^{\mathsf{T}} \quad \mathbf{v}_0^{\mathsf{T}} \quad \mathbf{m}^{\mathsf{T}}\,\right]^{\mathsf{T}}, \tag{20}$$

where $\mathbf{r}_0$ is the initial position of the target, $\mathbf{v}_0$ its constant velocity and $\mathbf{m}$ its constant magnetic dipole moment. Thus, the model (18) has 12 parameters where 6 of them enter linearly in (18) ($\mathbf{B}_0$ and $\mathbf{m}$) whereas the other 6 ($\mathbf{r}_0$ and $\mathbf{v}_0$) enter non-linearly.

In a similar manner also the extended target model presented in (10) can be reformulated under the constant velocity assumption. Here, all magnetic dipole moments $\mathbf{m}^{1:d}$ will be constant. We have

$$\mathbf{h}_{j,k}^d(\mathbf{x}) = \mathbf{B}_{0,j} + \sum_{i=1}^{d}\mathrm{J}^{\mathbf{m}}\left(\mathbf{r}_k + \Delta\mathbf{r}_k^i - \boldsymbol{\theta}_j\right)\mathbf{m}^i, \tag{21a}$$

with

$$\Delta\mathbf{r}_k^i = \left(i - \frac{d+1}{2}\right)\frac{L}{d-1}\frac{\mathbf{v}_0}{\|\mathbf{v}_0\|} \quad \text{and} \quad \mathbf{r}_k = \mathbf{r}_0 + kT_s\mathbf{v}_0. \tag{21b}$$

The total sensor model is then given by

$$\mathbf{y}_{j,k} = \mathbf{h}_{j,k}^d(\mathbf{x}) + \mathbf{e}_{j,k} \tag{21c}$$

$$\text{with}\quad \mathbf{x} = \left[\,(\mathbf{B}_{0,1:J})^{\mathsf{T}} \quad \mathbf{r}_0^{\mathsf{T}} \quad \mathbf{v}_0^{\mathsf{T}} \quad (\mathbf{m}^{1:d})^{\mathsf{T}} \quad L\,\right]^{\mathsf{T}}. \tag{21d}$$

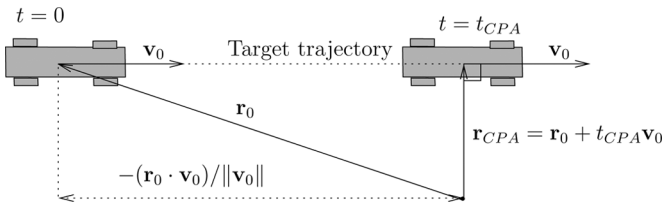

Fig. 3. The CPA time t_{CPA} and CPA range r_{CPA} can be expressed by the initial position $\mathbf{r}_0$ and the velocity $\mathbf{v}_0$.

B. Anderson Function Expansion for Constant Velocity

The presented sensor model (18) describes the observed magnetometer signal if the target is moving with constant velocity. An equivalent model [4], [6]–[8] for the same problem setup can be formulated by modeling the signal itself. Direct calculations [4] starting from (18) reveals that each of the three dimensions in the sensor response $\mathbf{y}_k$ can be expressed as a linear combination of three elementary functions. These functions are known as the Anderson functions [4]. By choosing the time origin at the closest point of approach (CPA) time t_{CPA} and normalizing it with the CPA range r_{CPA} and the speed $v_0 = \|\mathbf{v}_0\|$, the resulting model is

$$\mathbf{y}_k = \mathbf{B}_0 + \mathrm{C} \cdot \mathbf{f}\left(\frac{v_0}{r_{\mathrm{CPA}}}(kT_s - t_{\mathrm{CPA}})\right) + \mathbf{e}_k, \tag{22}$$

where the time dependency enters in the orthogonal Anderson functions [4]

$$\mathbf{f}(t) = [\, f_0(t) \quad f_1(t) \quad f_2(t)\,]^{\mathsf{T}} \tag{23a}$$

$$f_n(t) = \frac{t^n}{(t^2+1)^{\frac{5}{2}}}, \quad n = 0, 1, 2 \tag{23b}$$

and where C is a 3×3-matrix of coefficients. Consequently, (22) is linear in $\mathbf{B}_0$ and C, which includes $3 + 9 = 12$ parameters, and is nonlinear in the remaining 3 parameter v_0, r_{CPA} and t_{CPA}, in total 15 parameters.

Both t_{CPA} and r_{CPA} are related to the parameters in (20) in the following way: The traveled distance between $t = 0$ and $t = t_{\mathrm{CPA}}$ is equal to the projection of $-\mathbf{r}_0$ onto $\mathbf{v}_0$, see Fig. 3.

This gives the CPA time and CPA range

$$t_{\mathrm{CPA}} = -\frac{(\mathbf{r}_0 \cdot \mathbf{v}_0)}{\|\mathbf{v}_0\|} \Big/ \|\mathbf{v}_0\| = -\frac{(\mathbf{r}_0 \cdot \mathbf{v}_0)}{(\mathbf{v}_0 \cdot \mathbf{v}_0)} \tag{24a}$$

$$r_{\mathrm{CPA}} = \|\mathbf{r}_{\mathrm{CPA}}\| = \|\mathbf{r}_0 + t_{\mathrm{CPA}} \cdot \mathbf{v}_0\|. \tag{24b}$$

Furthermore, also the coefficients in C are related to (20) in that

$$\mathrm{C} = \beta[\, \mathbf{c}_1 \quad \mathbf{c}_2 \quad \mathbf{c}_3\,], \tag{25a}$$

with

$$\mathbf{c}_1 = 3(\tilde{\mathbf{r}} \cdot \tilde{\mathbf{m}})\tilde{\mathbf{r}} - \tilde{\mathbf{m}}, \tag{25b}$$

$$\mathbf{c}_2 = 3(\tilde{\mathbf{r}} \cdot \tilde{\mathbf{m}})\tilde{\mathbf{v}} - 3(\tilde{\mathbf{v}} \cdot \tilde{\mathbf{m}})\tilde{\mathbf{r}}, \tag{25c}$$

$$\mathbf{c}_3 = 3(\tilde{\mathbf{m}} \cdot \tilde{\mathbf{v}})\tilde{\mathbf{v}} - \tilde{\mathbf{m}}, \tag{25d}$$

where the following normalization has been used

$$\beta = \frac{\mu_0}{4\pi}\frac{m}{r_{\mathrm{CPA}}^3}, \quad \tilde{\mathbf{r}} = \frac{\mathbf{r}_{\mathrm{CPA}}}{r_{\mathrm{CPA}}}, \quad \tilde{\mathbf{v}} = \frac{\mathbf{v}_0}{v_0}, \quad \tilde{\mathbf{m}} = \frac{\mathbf{m}}{m}. \tag{26}$$

C. Comparison

By comparing the two different models (18) and (22), the following observations can be made

- The Anderson function model (22) consists of 15 parameters, whereas the dipole model (18) consists of only 12. Consequently, (22) is over-parametrized. The reason is that the superposition of the Anderson functions in (22) is nonlinearly constrained and does not have all 9 degrees of freedom as given in (22). This can be seen by inspecting (25). Each of the unit vectors $\tilde{\mathbf{r}}$, $\tilde{\mathbf{v}}$ and $\tilde{\mathbf{m}}$ contribute with 2 degrees of freedom to the matrix C. By taking the coefficient β and the constraint $(\tilde{\mathbf{r}} \cdot \tilde{\mathbf{v}}) = 0$ into account, C has in total only 6 independent components, or equivalently, the 9 coefficients in C have to obey 3 (non-linear) constraints. These constraints are not present in (22). Thus, (22) is a relaxation of (18).
- The dipole model (18) has 6 parameters entering non-linearly in the model, whereas (22) has only 3. Since the relaxation reduces the non-linearity, (22) can be seen as a convexification of the more non-linear model (18).
- The parametrization of (18) is directly related to the target trajectory ($\mathbf{r}_0$ and $\mathbf{v}_0$) and the magnetic signature of the target $\mathbf{m}$. This will make the multi sensor extension of (18) trivial, see Section II.B. In contrast, a multi sensor version of (22) has to rely on sub-optimal solutions where each sensor estimates its own matrix $\hat{\mathrm{C}}$, which then are fused at a later stage, as done in [8].
  In addition, (18) can easily be extended to tracking by applying a motion model and a nonlinear filter, which has been done in [11]. This extension would for (22) be harder, since the shape of the Anderson functions relies on a linear motion of the target.

IV. Magnetometer Potential for Localization and Tracking

In this section limitations and possibilities of the magnetometer will be discussed in terms of observability and the Cramér Rao lower bound as a function of the placement of a second sensor.

Without loss of generality the bias $\mathbf{B}_0$ is assumed to be known and the discussion will be based on the unbiased static sensor model in (18) with the state $\mathbf{x} = [\, \mathbf{r}_0^{\mathsf{T}} \quad \mathbf{v}_0^{\mathsf{T}} \quad \mathbf{m}^{\mathsf{T}}\,]^{\mathsf{T}}$ to make the analysis cleaner. We will therefore consider the model

$$\mathbf{h}_k(\mathbf{x}) = \frac{\mu_0}{4\pi}\frac{3(\mathbf{r}_k \cdot \mathbf{m})\mathbf{r}_k - \|\mathbf{r}_k\|^2\mathbf{m}}{\|\mathbf{r}_k\|^5}, \quad \text{where} \quad \mathbf{r}_k = \mathbf{r}_0 + kT_s\mathbf{v}_0. \tag{27}$$

A. Single Sensor Observability

To analyze observability, a local analysis can be performed. Consider the *Fisher information matrix* (FIM), which under Gaussian assumptions of the sensor noise $\mathbf{e}_k \sim \mathcal{N}(\mathbf{0}, \mathrm{R})$ reads

$$\mathcal{I}(\mathbf{x}^0) \triangleq \sum_{k=1}^{N} \nabla\mathbf{h}_k^{\mathsf{T}}(\mathbf{x}^0)\mathrm{R}^{-1}\nabla\mathbf{h}_k(\mathbf{x}^0), \tag{28}$$

where $\mathbf{x}^0$ are the true parameters. Any zero eigenvalues of this matrix makes it singular, which indicates a lack of local observability at $\mathbf{x}^0$. The unobservable subspace is spanned by the

eigenvectors corresponding to the zero eigenvalues, also known as the kernel of the matrix. Indeed, it can be shown that the kernel of $\mathcal{I}(\mathbf{x}^0)$ is at least of dimension one.

Proposition 1: Consider the sensor model (27) and its information matrix (28). Then

$$\mathcal{I}(\mathbf{x}^0)\cdot\begin{bmatrix}\mathbf{r}_0\\ \mathbf{v}_0\\ 3\mathbf{m}\end{bmatrix}=\mathbf{0},\quad \text{for all}\quad \mathbf{x}^0=\begin{bmatrix}\mathbf{r}_0\\ \mathbf{v}_0\\ \mathbf{m}\end{bmatrix}\in\mathbb{R}^9. \tag{29}$$

Proof: Define $\bar{\mathbf{x}}=[\,\mathbf{r}_0^{\mathsf{T}}\quad \mathbf{v}_0^{\mathsf{T}}\quad 3\mathbf{m}^{\mathsf{T}}\,]^{\mathsf{T}}$ and apply $\bar{\mathbf{x}}$ to the Jacobian

$$\begin{aligned}\nabla\mathbf{h}_k(\mathbf{x}^0)\bar{\mathbf{x}}&=[\,\mathrm{J}^{\mathbf{r}}(\mathbf{r}_k,\mathbf{m})\quad kT_s\mathrm{J}^{\mathbf{r}}(\mathbf{r}_k,\mathbf{m})\quad \mathrm{J}^{\mathbf{m}}(\mathbf{r}_k)\,]\cdot\begin{bmatrix}\mathbf{r}_0\\ \mathbf{v}_0\\ 3\mathbf{m}\end{bmatrix}\\ &=\mathrm{J}^{\mathbf{r}}(\mathbf{r}_k,\mathbf{m})\mathbf{r}_0+kT_s\mathrm{J}^{\mathbf{r}}(\mathbf{r}_k,\mathbf{m})\mathbf{v}_0+3\mathrm{J}^{\mathbf{m}}(\mathbf{r}_k)\mathbf{m}\\ &=\mathrm{J}^{\mathbf{r}}(\mathbf{r}_k,\mathbf{m})\mathbf{r}_k+3\mathrm{J}^{\mathbf{m}}(\mathbf{r}_k)\mathbf{m}.\end{aligned}$$

where $\mathrm{J}^{\mathbf{m}}(\mathbf{r}_k)$ and $\mathrm{J}^{\mathbf{r}}(\mathbf{r}_k,\mathbf{m})$ are the Jacobians of $\mathbf{h}_k(\mathbf{x})$ with respect to $\mathbf{m}$ and $\mathbf{r}_k$ and respectively

$$\mathrm{J}^{\mathbf{m}}(\mathbf{r}_k)=\frac{1}{\|\mathbf{r}_k\|^5}\left(3\mathbf{r}_k\mathbf{r}_k^{\mathsf{T}}-\|\mathbf{r}_k\|^2\mathrm{I}_3\right) \tag{30a}$$

$$\begin{aligned}\mathrm{J}^{\mathbf{r}}(\mathbf{r}_k,\mathbf{m})=\frac{3}{\|\mathbf{r}_k\|^5}\Big((\mathbf{r}_k\cdot\mathbf{m})\mathrm{I}_3+\mathbf{r}_k\mathbf{m}^{\mathsf{T}}\\ +\mathbf{m}\mathbf{r}_k^{\mathsf{T}}-5\frac{(\mathbf{r}_k\cdot\mathbf{m})}{(\mathbf{r}_k\cdot\mathbf{r}_k)}\mathbf{r}_k\mathbf{r}_k^{\mathsf{T}}\Big).\end{aligned} \tag{30b}$$

Further, we can show that

$$\mathrm{J}^{\mathbf{r}}(\mathbf{r}_k,\mathbf{m})\mathbf{r}_k=-3\mathrm{J}^{\mathbf{m}}(\mathbf{r}_k)\mathbf{m} \tag{31}$$

and from this we get

$$\nabla\mathbf{h}_k(\mathbf{x}^0)\bar{\mathbf{x}}=-3\mathrm{J}^{\mathbf{m}}(\mathbf{r}_k)\mathbf{m}+3\mathrm{J}^{\mathbf{m}}(\mathbf{r}_k)\mathbf{m}=\mathbf{0}\quad\forall k,$$

which leads to

$$\mathcal{I}(\mathbf{x}^0)\bar{\mathbf{x}}=\sum_{k=1}^{N}\nabla\mathbf{h}_k^{\mathsf{T}}(\mathbf{x}^0)\mathrm{R}^{-1}\underbrace{\nabla\mathbf{h}_k(\mathbf{x}^0)\bar{\mathbf{x}}}_{=\mathbf{0}}=\mathbf{0}.$$

■

Thus, the kernel is at least given by the following one-dimensional subspace:

$$\mathrm{Ker}(\mathcal{I}(\mathbf{x}^0))\supseteq\left(\lambda\,[\,\mathbf{r}_0^{\mathsf{T}}\quad\mathbf{v}_0^{\mathsf{T}}\quad 3\mathbf{m}^{\mathsf{T}}\,]^{\mathsf{T}}\,|\lambda\in\mathbb{R}\right). \tag{32}$$

In most cases the kernel dimension is exactly equal to one, meaning that (32) is fulfilled with equality. For example, for the following parameters $\mathbf{r}_0=[-3\quad 1\quad 0]^{\mathsf{T}}$, $\mathbf{v}_0=[1\quad 0\quad 0]^{\mathsf{T}}$ and $\mathbf{m}=[1\quad 1\quad 1]^{\mathsf{T}}$, the kernel of the information matrix indeed has dimension one. However, if $\mathbf{m}$ is orthogonal to both $\mathbf{r}_0$ and $\mathbf{v}_0$ the kernel will be larger. For example, for the parameter $\mathbf{r}_0=[-3\quad 1\quad 0]^{\mathsf{T}}$, $\mathbf{v}_0=[1\quad 0\quad 0]^{\mathsf{T}}$ and $\mathbf{m}=[0\quad 0\quad 1]^{\mathsf{T}}$ the kernel of the information matrix has dimension two.

Due to the non-linearity, the expression of the unobservable subspace (32) is only valid at the point $\mathbf{x}^0$ and can therefore only be regarded as the tangent of the unobservable one-dimensional manifold at this point. Denote this manifold $\tilde{\mathbf{x}}(u)=[\,\tilde{\mathbf{r}}_0(u)\quad\tilde{\mathbf{v}}_0(u)\quad\tilde{\mathbf{m}}(u)\,]^{\mathsf{T}}$, where u is a scalar parameter. For each u there will be a $\lambda(u)$ such that

$$\frac{d}{du}\tilde{\mathbf{x}}(u)=\frac{d}{du}\begin{bmatrix}\tilde{\mathbf{r}}_0(u)\\ \tilde{\mathbf{v}}_0(u)\\ \tilde{\mathbf{m}}(u)\end{bmatrix}=\lambda(u)\begin{bmatrix}\tilde{\mathbf{r}}_0(u)\\ \tilde{\mathbf{v}}_0(u)\\ 3\tilde{\mathbf{m}}(u)\end{bmatrix}. \tag{33}$$

By choosing the parametrization $u=\lambda(u)^{-1}$, we get the following unobservable manifold

$$\tilde{\mathbf{x}}(u)=\begin{bmatrix}u\mathbf{r}_0\\ u\mathbf{v}_0\\ u^3\mathbf{m}\end{bmatrix}. \tag{34}$$

It is instructive to substitute $\tilde{\mathbf{x}}(u)$ into (18) and conclude that $\mathbf{h}_{1:k}(\tilde{\mathbf{x}}(u))$ is independent of the parameter u, which means that all points on this manifold will give the same output $\mathbf{y}_k$. For example, multiplying $\mathbf{r}_0$ and $\mathbf{v}_0$ with 2, and $\mathbf{m}$ with $2^3=8$ will result in the same output $\mathbf{y}_k$.

The result is physically quite intuitive since the magnetometer does not measure any absolute distances and the system can be arbitrarily scaled without changing the measured output. Thus, a small vehicle driving slowly close to the sensor will give rise to the same signal as a large vehicle driving fast far from the sensor. Furthermore, the cubic scaling of the magnetic dipole moment $\mathbf{m}$ is reasonable since it is related to the volume of the vehicle.

The conducted observability analysis also gives insight to the comparison between the dipole model (18) and the Anderson function model (22):

- The sensor model (22) can easily be re-parametrized excluding the unobservable manifold (34) by introducing the scale parameter $\alpha=v_0/r_{\mathrm{CPA}}$. This parametrization has also been used in [4], [6]–[8]. An equivalent re-parametrization in (18) would inevitably increase the model complexity.
- By substituting (34) into (24a) it can be stated that t_{CPA} is independent of u and consequently observable. This means that t_{CPA} can be uniquely determined from only one vector magnetometer and does not necessarily need be aided with other sensors as done in [6]–[8] to achieve observability for that parameter. Furthermore, notice that only one axis of the vector magnetometer is sufficient to achieve observability for t_{CPA}. This can be seen by decomposing its signal into the three Anderson functions (23b), which each of them contains the information of t_{CPA}.

B. Single Sensor Observability With Prior Information

The lack of observability can be solved by using prior knowledge about the target trajectory. This situation has been studied in [6] and [7], which includes the possibility to use information about the range at CPA, for example by knowing the geometry of the road on which the vehicle is traveling. By using (24) this gives the extra scalar measurement

$$y_{\mathrm{CPA}}=h_{\mathrm{CPA}}(\mathbf{x}^0)=\|\mathbf{r}_{\mathrm{CPA}}\|=\left\|\mathbf{r}_0-\frac{(\mathbf{r}_0\cdot\mathbf{v}_0)}{(\mathbf{v}_0\cdot\mathbf{v}_0)}\cdot\mathbf{v}_0\right\| \tag{35}$$

and the corresponding information matrix can be computed as

$$\mathcal{I}_{\mathrm{CPA}}(\mathbf{x}^0)=\nabla h_{\mathrm{CPA}}^{\mathsf{T}}(\mathbf{x}^0)\alpha^{-1}\nabla h_{\mathrm{CPA}}(\mathbf{x}^0), \tag{36}$$

where $\alpha \to 0$ since the information in (24b) comes with zero uncertainty. Furthermore, since this prior knowledge is independent of the sensor information, the information matrices are additive, which gives

$$\mathcal{I}_{+\mathrm{CPA}}(\mathbf{x}^0) = \mathcal{I}(\mathbf{x}^0) + \mathcal{I}_{\mathrm{CPA}}(\mathbf{x}^0). \tag{37}$$

If the condition in (32) is fulfilled with equality, we only need to require that $\mathcal{I}_{\mathrm{CPA}}(\mathbf{x}^0) \cdot [\,\mathbf{r}_0^\mathsf{T} \quad \mathbf{v}_0^\mathsf{T} \quad 3\mathbf{m}^\mathsf{T}\,]^\mathsf{T} \neq \mathbf{0}$ for $\mathcal{I}_{+\mathrm{CPA}}(\mathbf{x}^0)$ to have full rank. This is indeed true if $\mathbf{r}_0$ is not parallel to $\mathbf{v}_0$.

Proposition 2: Consider the sensor model (35) and its information matrix (36). Then

$$\mathcal{I}_{\mathrm{CPA}}(\mathbf{x}^0) \cdot \begin{bmatrix} \mathbf{r}_0 \\ \mathbf{v}_0 \\ 3\mathbf{m} \end{bmatrix} = \mathbf{0} \tag{38}$$

if and only if $\mathbf{r}_0$ is parallel to $\mathbf{v}_0$.

Proof: Define $\bar{\mathbf{x}} = [\,\mathbf{r}_0^\mathsf{T} \quad \mathbf{v}_0^\mathsf{T} \quad 3\mathbf{m}^\mathsf{T}\,]^\mathsf{T}$ and apply $\bar{\mathbf{x}}$ to the Jacobian

$$\nabla h_{\mathrm{CPA}}(\mathbf{x}^0)\bar{\mathbf{x}} = \begin{bmatrix} \frac{\mathbf{r}_{\mathrm{CPA}}^\mathsf{T}}{\|\mathbf{r}_{\mathrm{CPA}}\|} & \frac{(\mathbf{r}_0 \cdot \mathbf{v}_0)\mathbf{r}_{\mathrm{CPA}}^\mathsf{T}}{(\mathbf{v}_0 \cdot \mathbf{v}_0)\|\mathbf{r}_{\mathrm{CPA}}\|} & \mathbf{0}_{1\times 3} \end{bmatrix} \cdot \begin{bmatrix} \mathbf{r}_0 \\ \mathbf{v}_0 \\ 3\mathbf{m} \end{bmatrix}$$

Since $(\mathbf{r}_{\mathrm{CPA}} \cdot \mathbf{v}_0) = 0$ we have

$$\begin{aligned} \nabla h_{\mathrm{CPA}}(\mathbf{x}^0)\bar{\mathbf{x}} &= \frac{(\mathbf{r}_{\mathrm{CPA}} \cdot \mathbf{r}_0)}{\|\mathbf{r}_{\mathrm{CPA}}\|} \\ &= \frac{(\mathbf{r}_0 \cdot \mathbf{r}_0)(\mathbf{v}_0 \cdot \mathbf{v}_0) - (\mathbf{r}_0 \cdot \mathbf{v}_0)(\mathbf{r}_0 \cdot \mathbf{v}_0)}{(\mathbf{v}_0 \cdot \mathbf{v}_0)\|\mathbf{r}_{\mathrm{CPA}}\|} \geq 0 \end{aligned}$$

and is only fulfilled with equality if and only if $\mathbf{r}_0$ is parallel to $\mathbf{v}_0$. This leads to

$$\mathcal{I}_{\mathrm{CPA}}(\mathbf{x}^0)\bar{\mathbf{x}} = \sum_{k=1}^{N} \nabla h_{\mathrm{CPA}}^\mathsf{T}(\mathbf{x}^0)\mathrm{R}^{-1}\nabla h_{\mathrm{CPA}}(\mathbf{x}^0)\bar{\mathbf{x}} = \mathbf{0}$$

if and only if $\mathbf{r}_0$ is parallel to $\mathbf{v}_0$. ∎

Consequently, we do not achieve observability if $\mathbf{r}_0$ is parallel to $\mathbf{v}_0$, which corresponds to $\mathbf{r}_{\mathrm{CPA}} = \mathbf{0}$. However, this situation can be considered as unphysical, since it would correspond to a scenario where the sensor is on the target trajectory.

C. Multi Sensor Observability

The lack of observability can also be solved with a second sensor. To handle multiple sensors, the sensor model has to be slightly expanded. Let the jth sensor be positioned at $\boldsymbol{\theta}_j$. The target parameter relative to the jth sensor will then be $\mathbf{x}_j = [\,(\mathbf{r}_0 - \boldsymbol{\theta}_j)^\mathsf{T} \quad \mathbf{v}_0^\mathsf{T} \quad \mathbf{m}^\mathsf{T}\,]^\mathsf{T}$ and the total sensor model is given by

$$\mathbf{y}_{k,j} = \mathbf{h}_k(\mathbf{x}_j) + \mathbf{e}_{k,j}, \quad \text{for all } j \in J. \tag{39}$$

Furthermore, under the assumption that the measurement noise of different sensors are independent, the information matrices for all sensors are additive, which gives

$$\mathcal{I}_J(\mathbf{x}^0, \boldsymbol{\theta}_{1:J}) = \sum_{j=1}^{J} \mathcal{I}(\mathbf{x}_j^0) \tag{40}$$

By again using Proposition 1 we have

$$\mathrm{Ker}\left(\mathcal{I}\left(\mathbf{x}_j^0\right)\right) \supseteq \left(\lambda\,[\,(\mathbf{r}_0 - \boldsymbol{\theta}_j)^\mathsf{T} \quad \mathbf{v}_0^\mathsf{T} \quad 3\mathbf{m}^\mathsf{T}\,]^\mathsf{T} \,|\, \lambda \in \mathbb{R}\right). \tag{41}$$

Assume that (41) is fulfilled with equality for two different sensors at $\boldsymbol{\theta}_1$ and $\boldsymbol{\theta}_2$. Then the intersection of their kernels will be empty if $\boldsymbol{\theta}_1 \neq \boldsymbol{\theta}_2$. Under these assumptions we will then reach observability for a system with two sensors.

D. Comparison

We can now compare two extensions from the single sensor setup

- Setup 1) One sensor with prior knowledge of CPA range
- Setup 2) Two sensors

Both scenarios resolve the observability issue reported for the single sensor setup except for some cases with special geometry. However, Setup 2 requires that both coordinate systems of the two sensors are aligned with each other and also that their relative position is known in order not to violate the sensor model (39). This issue is less critical in Setup 1 since any misalignment of the single sensor will not change the range to the target and will thus not violate the sensor model. Furthermore, in Setup 2 the two sensors need to be synchronized.

E. Cramér Rao Lower Bound

So far we have only compared the models concerning their observability properties. However, in order to find a good sensor deployment we want to quantify the best achievable estimation performance as a function of the sensor positions. This analysis is justified with the CRLB [23], which states that any unbiased estimate must have a covariance matrix larger than or equal to the inverse of the FIM

$$\mathrm{Cov}(\hat{\mathbf{x}}) - \mathcal{I}(\mathbf{x}^0)^{-1} \succeq 0. \tag{42}$$

The design goal in the sensor deployment is then to make the inverse of the information matrix as small as possible in order to minimize the covariance of the estimate. We do this analysis for the partitions of the state space corresponding to $\mathbf{r}_0$, $\mathbf{v}_0$ and $\mathbf{m}$ separately. We notice that for a positive semidefinite matrix any diagonal sub matrix is also positive semidefinite. By following [23] and using that property on (42) we get

$$[\mathrm{Cov}(\hat{\mathbf{x}}) - \mathcal{I}(\mathbf{x}^0)^{-1}]_{ii} \succeq 0 \tag{43}$$

and consequently

$$\mathrm{Cov}(\hat{\mathbf{x}}_i) = [\mathrm{Cov}(\hat{\mathbf{x}})]_{ii} \succeq [\mathcal{I}(\mathbf{x}^0)^{-1}]_{ii} \tag{44}$$

where i corresponds to a partition of the state vector. The design goal in the sensor deployment is then to minimize any of the three criteria

$$\|[\mathcal{I}(\mathbf{x}^0)^{-1}]_{\mathbf{r}_0\mathbf{r}_0}\|_2, \|[\mathcal{I}(\mathbf{x}^0)^{-1}]_{\mathbf{v}_0\mathbf{v}_0}\|_2, \|[\mathcal{I}(\mathbf{x}^0)^{-1}]_{\mathbf{m}\mathbf{m}}\|_2 \tag{45}$$

depending on if we are interested in a good estimation performance for the position $\mathbf{r}_0$, velocity $\mathbf{v}_0$ or magnetic dipole moment $\mathbf{m}$. In order to examine where a second magnetometer should be placed, these three criteria can be computed for different positions $\boldsymbol{\theta}_2$ of the second sensor. In [10] similar criteria

has been analyzed. For most values $\mathbf{x}^0$ the conclusion is that you should deploy a two sensor system symmetrically at both sides of the target trajectory if a good estimation performance for the position $\mathbf{r}_0$ and magnetic dipole moment $\mathbf{m}$ is of interest. On the other hand, for the velocity $\mathbf{v}_0$ it is better to place both sensors at the same side of the target trajectory and as separate as possible, which is intuitive. In the experiment presented in this work, the first of these two deployments has been considered.

V. Estimation

As already mentioned, in this work special interest will be given to scenarios where vehicles pass the sensors with constant velocity. Therefore, in this section the estimation methods to be used with the constant velocity models presented in Section III will be given. These methods will later be used in the sensor model validation presented in Section VI.

A. Sensor Noise Covariance

First, the distribution of the sensor noise $\mathbf{e}_{j,k}$ will be estimated for each of the magnetometers. According to [24], the noise of the magnetometer [25] is white Gaussian, i.e., its samples are i.i.d. and normally distributed with zero mean. Such a stochastic process is uniquely defined by its covariance matrix R. This matrix can be estimated from a measurement sequence without any moving targets by using the sample covariance

$$\mathrm{R}_j = \frac{1}{N-1}\sum_{k=1}^{N}(\mathbf{y}_{j,k}-\bar{\mathbf{y}}_j)(\mathbf{y}_{j,k}-\bar{\mathbf{y}}_j)^{\mathsf{T}}, \quad \text{where}$$
$$\bar{\mathbf{y}}_j = \frac{1}{N}\sum_{k=1}^{N}\mathbf{y}_{j,k}.$$

Here R_j represents the covariance of the jth sensor.

B. Parameter Estimation Using Constant Velocity Model

The parameter $\mathbf{x}$ introduced in the models (3) and (16) can be estimated using weighted least square by minimizing the cost function

$$\hat{\mathbf{x}} = \arg\min_{\mathbf{x}} V^d(\mathbf{x}) \tag{46a}$$
$$V^d(\mathbf{x}) = \sum_{k=1}^{N}\sum_{j=1}^{J}(\mathbf{y}_{j,k}-\mathbf{h}^d_{j,k}(\mathbf{x}))^{\mathsf{T}}\mathrm{R}_j^{-1}(\mathbf{y}_{j,k}-\mathbf{h}^d_{j,k}(\mathbf{x})). \tag{46b}$$

Note that under the Gaussian assumption of the measurement noise $\mathbf{e}_{j,k}$, (46) will be both a *minimum variance* and a *maximum likelihood* estimate.

In this framework, also the covariance of the estimate $\hat{\mathbf{x}}$ can be estimated. The covariance can be approximated as [26]

$$\mathrm{Cov}(\hat{\mathbf{x}}) \approx \left(\sum_{k=1}^{N}\sum_{j=1}^{2}\nabla\mathbf{h}^d_{j,k}(\hat{\mathbf{x}})^{\mathsf{T}}\mathrm{R}_j^{-1}\nabla\mathbf{h}^d_{j,k}(\hat{\mathbf{x}})\right)^{-1}. \tag{47}$$

which can be derived from a second order approximation of the cost function (46b), where we use that $\nabla V^d(\mathbf{x})|_{\mathbf{x}=\hat{\mathbf{x}}} = \mathbf{0}$ at optimum.

C. Model Validation

The number of dipoles d can for this model class be considered as a model order parameter, which will affect the statistical properties of the cost function. Under the assumption that both the measurement equation $\mathbf{h}_{j,k}(\mathbf{x})$ and the noise $\mathbf{e}_{j,k} \sim \mathcal{N}(\mathbf{0}, \mathrm{R}_j)$ are correctly modeled, the cost function $V^d(\hat{\mathbf{x}})$ will be $\chi^2_{Nn_y-n_x}$ distributed, n_y and n_x being the dimension of each measurement and the state space respectively. For the extended target model in (16) this will be

$$n_y = \dim(\mathbf{y}_{1:J,k}) = 3J \tag{48}$$
$$n_x = \dim\left([\,(\mathbf{B}_{0,1:J})^{\mathsf{T}} \quad \mathbf{r}_0^{\mathsf{T}} \quad \mathbf{v}_0^{\mathsf{T}} \quad (\mathbf{m}^{1:d})^{\mathsf{T}} \quad L\,]^{\mathsf{T}}\right)$$
$$= 3J+3+3+3d+1 = 3J+7+3d. \tag{49}$$

Since the mean of $\chi^2_{Nn_y-n_x}$ is equal to Nn_y-n_x, the normalized cost function

$$\bar{V}^d(\hat{\mathbf{x}}) = V^d(\hat{\mathbf{x}})/(Nn_y-n_x)$$
$$= V^d(\hat{\mathbf{x}})/(3NJ-3J-7-3d) \tag{50}$$

is considered and $\bar{V}^d(\hat{\mathbf{x}}) \approx 1$ would indicate a correct model. Therefore, the normalized cost function can be used for choosing an appropriate model order. However, in this work no explicit model order selection rule will be proposed.

D. State and Parameter Estimation

By using the maneuvering target model presented in Section II.E, the constant velocity assumption can be relaxed. By combining that sensor model with an appropriate motion model, a non-linear filter can be applied to estimate all states included in the model. Related results have been reported in [11] where a (nearly) constant velocity model has been applied and the estimation has been performed with an Extended Kalman Filter using data for vehicles passing a three-way intersection.

VI. Sensor Model Validation

In order to validate the proposed sensor models, real experimental data has been collected with magnetometers contained in commercial-grade measurement units [25]. In this section, the experimental setup will be described and the results of the validation will be given using the estimation methodology presented in Section V. In accordance with the results in Section IV.A and IV.C, all measurements have been done with two sensors in order to reach observability.

A. Experimental Setup

The two magnetometers have been placed close to a straight road (see Fig. 4). In accordance with the discussion in Section IV.E they have been deployed symmetrically at each side of the road. In the experimental setup a relative distance of 9.0 m between the sensors has been used. As reference data a video camera has been used recording all objects within the sensor range area. Data from six vehicles (Fig. 5) passing the sensors are used for the sensor model validation in Section VI.C and VI.D.

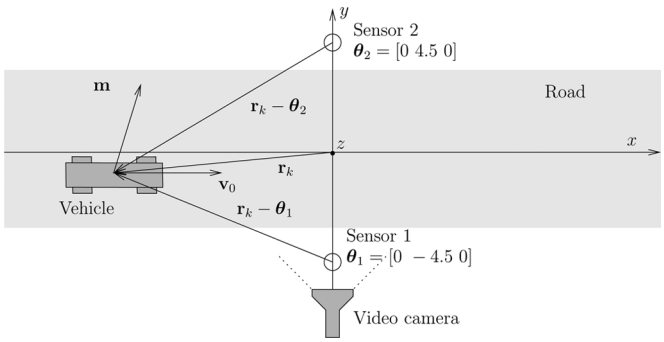

Fig. 4. Sensor setup for the sensor model validation. $\mathbf{r}_k$ is a vector from the origin to the vehicle, $\mathbf{v}_0$ is the velocity of the vehicle, $\mathbf{m}$ is the magnetic moment of the vehicle and $\boldsymbol{\theta}_1$ and $\boldsymbol{\theta}_2$ are the positions of the two sensors.

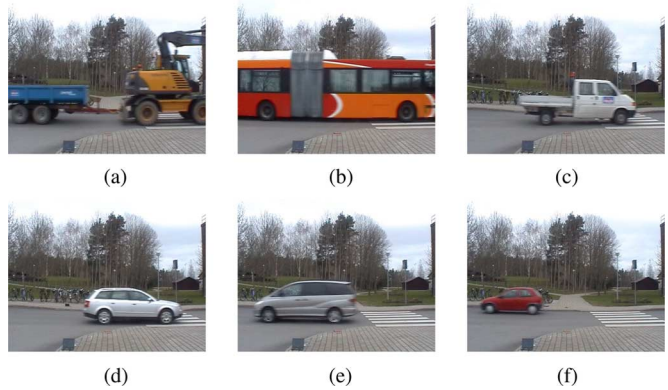

Fig. 5. The vehicles used in the sensor model validation. (a) Vehicle 1, (b) Vehicle 2, (c) Vehicle 3, (d) Vehicle 4, (e) Vehicle 5, (f)Vehicle 6.

B. Sensor Noise Covariance

Without any targets, each magnetometer measures a stationary magnetic field together with sensor noise. This stationary magnetic field mainly consists of the earth magnetic field but also of induced magnetic fields from other stationary ferromagnetic objects in the environment. We do not need to assume that the magnetic field in the environment is homogeneous, however we do assume it to be stationary.

By using data from a time window without any moving targets present, the sensor noise covariance can be estimated using the approach described in Section V.A. In this manner, the two symmetric 3×3-matrices R_1 and R_2 for the two sensors in use are estimated to be

$$\mathrm{R}_1 = 10^{-15} \begin{bmatrix} 0.1303 & -0.0073 & -0.0114 \\ -0.0073 & 0.1112 & 0.0117 \\ -0.0114 & 0.0117 & 0.1558 \end{bmatrix}, \quad (51a)$$

$$\mathrm{R}_2 = 10^{-15} \begin{bmatrix} 0.1500 & 0.0205 & 0.0215 \\ 0.0205 & 0.1937 & 0.0310 \\ 0.0215 & 0.0310 & 0.1483 \end{bmatrix}, \quad (51b)$$

where the unit of the measurement is Tesla.

C. Point Target Model Validation

Since the road is straight, the constant velocity assumption for all vehicles applies. We start with modeling the vehicles as a single dipole. Since we have a scenario with multiple sensors, the sensor model presented in II.B will be considered.

In Table I the normalized cost function for the vehicles in Fig. 5 is presented. By this we can conclude that larger vehicles generally produce a worse fit with the measured data than smaller vehicles do. This is intuitively clear since the point target model assumes that the target has no geometrical extension, which is a more rough approximation for large vehicles than for small vehicles. However, for all vehicles, the normalized cost function is much larger than 1.

Finally, by simulating the model with the estimated parameter $\hat{\mathbf{x}}$ we get an estimate of the measured quantity $\hat{\mathbf{y}}_{j,k} = \mathbf{h}_{j,k}(\hat{\mathbf{x}})$, which can be compared with the measured magnetic field $\mathbf{y}_{j,k}$. Note that the residual $\|\mathbf{y}_{j,k} - \hat{\mathbf{y}}_{j,k}\|_{\mathrm{R}_j}$ is exactly what is being minimized in the nonlinear least squares framework. In Fig. 6(a) the estimated x-component of the magnetic field for sensor 1, $\hat{y}^{\mathsf{x}}_{j=1,k}$, is compared with its measured equivalence $y^{\mathsf{x}}_{j=1,k}$. We can see that the main character of the signal has been caught. However, there is potential to get a better fit.

TABLE I
THE VALUES OF THE NORMALIZED COST FUNCTION $V^1(\hat{\mathbf{x}})/(Nn_y - n_x)$ FOR THE POINT TARGET MODEL $d = 1$. N IS NUMBER OF SAMPLES, n_y THE DIMENSION OF EACH MEASUREMENT AND n_x THE STATE DIMENSION

Vehicle	$V^1(\hat{\mathbf{x}})/(Nn_y - n_x)$	N	n_y	n_x
1	360	70	6	15
2	142	54	6	15
3	10	32	6	15
4	14	44	6	15
5	51	27	6	15
6	17	22	6	15

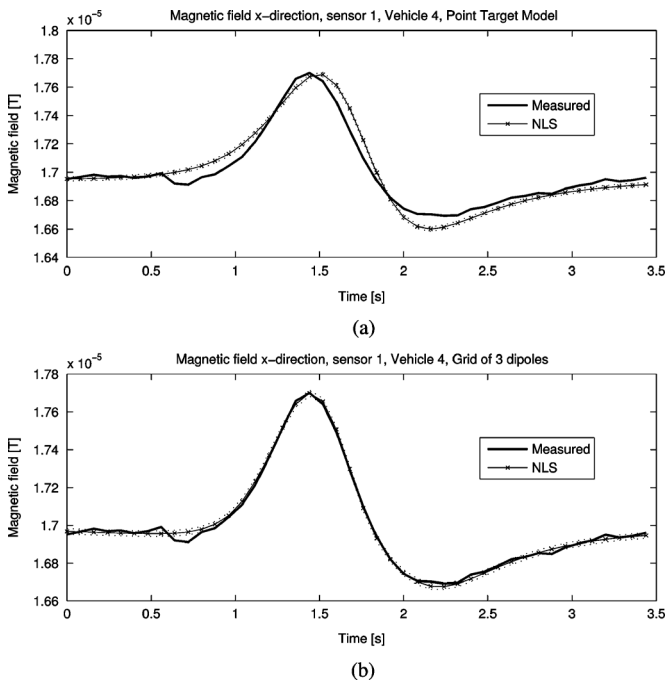

Fig. 6. The measured magnetic field $y^{\mathsf{x}}_{j=1,k}$ in the x-direction, and the estimated value $h^{\mathsf{x}}_{j=1,k}(\hat{\mathbf{x}})$ using nonlinear least squares (NLS) for vehicle 4 with a 90% confidence interval. (a) The point target model with one dipole, (b) The extended target model with a row of three dipoles.

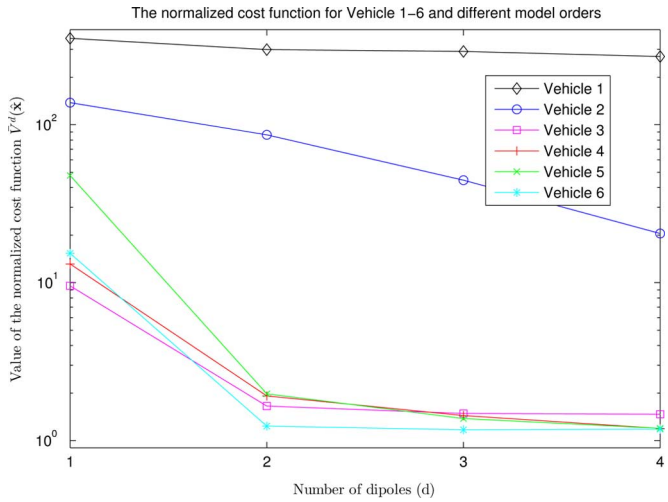

Fig. 7. The normalized cost function $\bar{V}^d(\hat{\mathbf{x}})$ as a function of the model order d of the extended target model.

TABLE II
THE NORMALIZED COST FUNCTION FOR THE EXTENDED TARGET MODEL $d = 3$ AND THE ESTIMATED LENGTH BETWEEN THE FIRST AND THE LAST DIPOLE WITH THE CORRESPONDING STANDARD DEVIATION

Nr	$V^3(\hat{\mathbf{x}})/(Nn_y - n_x)$	N	n_y	n_x	Length [m]	
1	302.6	70	6	22	9.09	(0.03)
2	76.7	54	6	22	11.25	(0.04)
3	1.6	32	6	22	3.95	(0.36)
4	1.5	44	6	22	3.56	(0.15)
5	1.5	27	6	22	4.98	(0.25)
6	1.3	22	6	22	2.07	(0.24)

D. Extended Target Model Validation

In order to improve the model fit, the extended target model (16) with $d > 1$ will considered.

1) Model Order Selection and Model Validation: For an extended target model, an arbitrary model order can be chosen which here is the number of dipoles d. In Fig. 7, the normalized cost function (50) is displayed as a function of the model order d.

For most vehicles, the normalized cost function rapidly decreases with higher model order d. For the smaller vehicles it can be seen that the normalized cost function converges towards 1, which corresponds to a correct model.

With the model order $d = 3$, the equivalent plot to Fig. 6(a) can be found in Fig. 6(b). From this it can be concluded that an almost perfect fit has been achieved. This model order will be used for a more thorough analysis and all results are presented in Tables II, III, IV and V for each vehicle.

In Table II the normalized cost function for the vehicles is given. We have seen that this quantity should equal 1 for correct models. By comparing Table II with Table I, we see that the small vehicles 3–6 have taken huge steps in this direction, whereas the large vehicles 1–2 still have a long way to go. This faces the real difficulties finding feasible models for large vehicles using models with a reasonable state space dimension.

2) Length Estimation: Extended target models also produce new states, where length of the row of dipoles has a direct physical interpretation. The estimate of this length is also presented in Table II and do correspond to the size of the vehicles given in Fig. 5. Notice that this length does not exactly correspond to the actual length of the vehicle since it is based on an approximation of the target using a finite number of dipoles. However, a long dipole row should indicate a long vehicle and vise versa, which then might be used for classifying vehicles of different sizes.

TABLE III
THE ESTIMATED INITIAL POSITION $\hat{\mathbf{r}}_0$ IN CARTESIAN COORDINATES (xyz) FOR THE EXTENDED TARGET MODEL $d = 3$. STANDARD DEVIATIONS IN PARENTHESIS. ALSO REFERENCE DATA FOR THE THREE CARTESIAN COORDINATES IS GIVEN. FOR EXAMPLE, FOR VEHICLE 1 THE x-COMPONENT OF $\hat{\mathbf{r}}_0$ IS -12.47 M WITH A STANDARD DEVIATION OF 0.04 M AND ACCORDING TO THE REFERENCE DATA THIS PARAMETER SHOULD BE NEGATIVE

Nr	Estimated initial position $\hat{\mathbf{r}}_0$ [m]						Ref. data		
1	-12.47,	0.13,	4.36	(0.04,	0.02,	0.04)	-,	0,	+
2	13.68,	-0.21,	0.32	(0.06,	0.03,	0.05)	+,	0,	+
3	-10.49,	-1.47,	0.57	(0.27,	0.09,	0.09)	-,	0,	+
4	-8.73,	-2.00,	0.25	(0.14,	0.08,	0.07)	-,	0,	+
5	11.43,	-1.47,	0.59	(0.20,	0.10,	0.10)	+,	0,	+
6	8.78,	0.93,	0.42	(0.22,	0.14,	0.09)	+,	0,	+

TABLE IV
THE ESTIMATED VELOCITY $\hat{\mathbf{v}}_0$ IN CARTESIAN COORDINATES (xyz) FOR THE EXTENDED TARGET MODEL $d = 3$. STANDARD DEVIATIONS IN PARENTHESIS. ALSO REFERENCE DATA IS GIVEN

Nr	Estimated velocity $\hat{\mathbf{v}}_0$ [m/s]						Ref. data		
1	6.41,	-0.27,	-1.54	(0.02,	0.01,	0.02)	+,	0,	0
2	-5.98,	0.20,	0.28	(0.03,	0.01,	0.02)	-,	0,	0
3	7.37,	0.33,	0.21	(0.16,	0.06,	0.06)	+,	0,	0
4	5.34,	0.28,	0.20	(0.08,	0.05,	0.04)	+,	0,	0
5	-9.74,	0.34,	0.02	(0.15,	0.09,	0.08)	-,	0,	0
6	-11.56,	1.18,	0.03	(0.25,	0.19,	0.11)	-,	0,	0

TABLE V
THE VALUES OF THE ESTIMATED TOTAL MAGNETIC MOMENT $\hat{\mathbf{m}} = \sum_{i=1}^{d} \hat{\mathbf{m}}^i$ IN CARTESIAN COORDINATES (xyz) FOR THE EXTENDED TARGET MODEL $d = 3$. STANDARD DEVIATIONS IN PARENTHESIS. ALSO REFERENCE DATA FOR THE THREE CARTESIAN COORDINATES IS GIVEN

Nr	Estimated magnetic dipole moment $\hat{\mathbf{m}}$ [Am^2]						$\|\hat{\mathbf{m}}\|$	Rf.
1	25,	-819,	-1528	(10,	5,	10)	1734	Large
2	305,	62,	-1872	(12,	5,	12)	1897	Large
3	-22,	-5,	-580	(8,	5,	13)	581	Small
4	-129,	-71,	-430	(8,	5,	12)	454	Small
5	-142,	142,	-438	(8,	7,	13)	482	Small
6	195,	-62,	-265	(10,	7,	19)	335	Small

3) Initial State and Velocity Estimation: Furthermore, the extended target model produces reasonable estimates of the initial position $\hat{\mathbf{r}}_0$, Table III, and the velocity $\hat{\mathbf{v}}_0$, Table IV. All target trajectories are almost parallel to the x-axis in accordance with the experimental setup. Furthermore, Vehicle 1, 3 and 4 are estimated to head in positive x-direction (right) (see Table IV), which is correct according to Fig. 5.

4) Height Estimation: The z-component of the initial position $\hat{\mathbf{r}}_0$ has the interpretation of being the height of the car's metallic center over the road plane. According to Table III this estimate is reasonable, being positive for all vehicles and significantly larger for Vehicle 1.

5) Dipole Estimation: Finally, by making use of the superposition principle (9), the total magnetic dipole moment of the vehicles can be calculated by summarizing all dipoles. This estimate is given in Table V. However, for these values we do not have any reference data more than that large $\hat{\mathbf{m}}$ should correspond to large vehicles.

TABLE VI
THE ESTIMATED HARD IRON DIPOLE MOMENT $\hat{\mathbf{r}}_0$ IN CARTESIAN COORDINATES (xyz) AND ESTIMATED SOFT IRON SCALAR $\hat{D}$. STANDARD DEVIATIONS IN PARENTHESIS

Estimated hard iron dipole moment $\hat{\mathbf{m}}_0$ [Am^2]						$\hat{D}$ [m^3]	
-203,	124,	-267	(2.1,	1.7,	4.9)	1.054	(0.011)

E. Validation of Direction Dependent Target Model

The proposal of decomposing the magnetic dipole moment $\mathbf{m}$ into two components as described in (15) cannot be validated from one scenario with constant heading since the two components cannot be resolved. As stated in [5], different observations of the same target at multiple headings are needed to allow the induced and permanent dipole moments to be resolved. In this validation, Vehicle 5, Fig. 5(e), has been used in controlled experiments heading at different speeds in four different directions, 2–4 times in each direction.

For each scenario the corresponding $\hat{\mathbf{m}}(\Psi)$ has been estimated with the row of dipoles extended target model with model order $d = 3$, which in Section VI.D has been proved to be a good model. Now we define

$$\mathbf{Y} = \begin{bmatrix} \hat{\mathbf{m}}(\Psi_1) \\ \hat{\mathbf{m}}(\Psi_2) \\ \vdots \\ \hat{\mathbf{m}}(\Psi_i) \\ \vdots \\ \hat{\mathbf{m}}(\Psi_n) \end{bmatrix}, \Phi^{\mathsf{T}} = \begin{bmatrix} \mathrm{Q}(\Psi_1) & \mathbf{B}_0/\mu_0 \\ \mathrm{Q}(\Psi_2) & \mathbf{B}_0/\mu_0 \\ & \vdots \\ \mathrm{Q}(\Psi_i) & \mathbf{B}_0/\mu_0 \\ & \vdots \\ \mathrm{Q}(\Psi_n) & \mathbf{B}_0/\mu_0 \end{bmatrix}, \boldsymbol{\theta} = \begin{bmatrix} \mathbf{m}_0 \\ D \end{bmatrix},$$

$$\mathrm{R} = \begin{bmatrix} \mathrm{Cov}(\hat{\mathbf{m}}(\Psi_1)) & & \mathbf{0} \\ & \ddots & \\ \mathbf{0} & & \mathrm{Cov}(\hat{\mathbf{m}}(\Psi_n)) \end{bmatrix},$$

where i are the different scenarios performed at heading angle Ψ_i. The weighted least squares estimate of $\boldsymbol{\theta}$ can be found by minimizing the residual $\|\mathbf{Y} - \Phi^{\mathsf{T}}\hat{\boldsymbol{\theta}}\|_{\mathrm{R}}$, i.e., by solving

$$(\Phi \mathrm{R}^{-1}\Phi^{\mathsf{T}})\hat{\boldsymbol{\theta}} = \Phi \mathrm{R}^{-1}\mathbf{Y}$$

with the corresponding covariance matrix

$$\mathrm{P} = (\Phi \mathrm{R}^{-1}\Phi^{\mathsf{T}})^{-1}.$$

The estimated parameter $\hat{\boldsymbol{\theta}} = \begin{bmatrix} \hat{\mathbf{m}}_0 \\ \hat{D} \end{bmatrix}$ are given in Table VI together with their standard deviations $\sqrt{P_{ii}}$.

In order to validate (15), predictions of the magnetic dipole moment $\mathbf{m}$ for new Ψ can be made by using $\hat{\mathbf{m}}_0$ and $\hat{D}$

$$\hat{\hat{\mathbf{m}}}(\Psi) = \mathrm{Q}(\Psi)\hat{\mathbf{m}}_0 + \frac{\hat{D}}{\mu_0}\mathbf{B}_0. \tag{52}$$

The predictions can be compared with the previously estimated $\hat{\mathbf{m}}(\Psi_i)$. In Fig. 8 the excellent fit for the x-and y-component of $\hat{\mathbf{m}}(\Psi_i)$ and $\hat{\hat{\mathbf{m}}}(\Psi_i)$ is displayed.

By this it can be verified that the magnetic dipole moment $\mathbf{m}$ can be decomposed into two components: one being parallel to the earth magnetic field with the scalar multiplier D/μ_0, and one being oriented in the reference frame of the vehicle $\mathbf{m}_0$ where the parameters $\mathbf{m}_0$ and D are vehicle specific. Note that $\mathbf{m}_0$ and D cannot be found only from a single measurement since $\hat{\mathbf{m}}(\Psi)$ contains three components whereas $\mathbf{m}_0$ and D in total contains four. In other words, the target needs to make maneuvers in order to excite its complete magnetic signature.

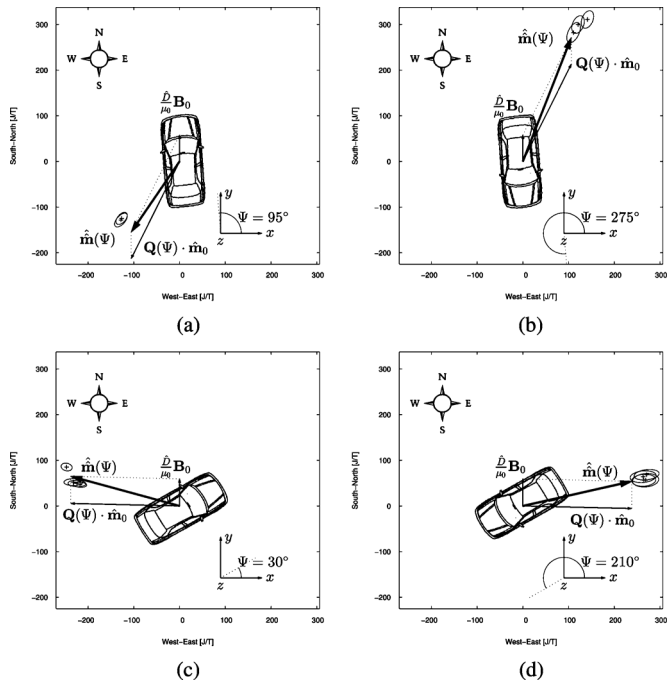

Fig. 8. The estimated magnetic dipole moments $\hat{\mathbf{m}}(\Psi)$ (the crosses) for different heading angles Ψ given with a 90% confidence interval (the small ellipses) together with the simulated $\hat{\hat{\mathbf{m}}}(\Psi)$ using the estimated parameter. The magnetic dipole moment can successfully be divided into two components, one being parallel to the earth magnetic field, and one being oriented in the reference frame of the vehicle. (a) Vehicle 5 heading north., (b) Vehicle 5 heading south. (c) Vehicle 5 heading north-east. (d) Vehicle 5 heading south-west.

VII. CONCLUSION

In this paper, we have addressed the problem of localizing metallic targets using magnetometers. We have presented a general sensor model based on the magnetic dipole model. This model has been extended by introducing a model consisting of a series of dipoles, which also contains the length of the vehicle in an extended state vector. Also a new model with heading angle dependent dipole moments has been proposed, which has been accomplished by decomposing the influence of soft and hard iron. The sensor model allows the target to be observed in an arbitrary magnetometer network.

We have also provided a detailed observability analysis of the model and compared it to other models based on the so called Anderson functions in the closest related papers. We have also provided measures for analyzing the optimal sensor deployment in a magnetometer sensor network using criteria based on the Cramér Rao lower bound.

Further, our model has been validated with a selection of dedicated field experiments. It has been found that the natural single dipole model cannot be validated for vehicles close to the sensor when a commercial-grade sensor is used in its field of coverage. It has been found that this extended target model works excellently on small vehicles. However, for large vehicles close to the sensor challenging modeling work still remains. Finally, target orientation dependent dipole moments are identifiable only if

the vehicle is observed in different orientations. Therefore, this model has been validated using the same vehicle in controlled experiments heading in different directions with good results. In addition, these experiments also verify that the dipole vectors are reproducible for a certain vehicle.

REFERENCES

[1] J. D. Jackson, *Classical Electrodynamics*, 3rd ed. New York, NY, USA: Wiley, 1999.

[2] J. Lenz, "A review of magnetic sensors," *Proc. IEEE*, vol. 78, pp. 973–989, Jun. 1990.

[3] J. Lenz and S. Edelstein, "Magnetic sensors and their applications," *IEEE Sensors J.*, vol. 6, no. 3, pp. 631–649, Jun. 2006.

[4] W. M. Wynn, "Detection, localization, and characterization of static magnetic dipole sources," in *Detection and Identification of Visually Obscured Targets*. New York, NY, USA: Taylor & Francis, 1999.

[5] J. W. Casalegno, "All-weather vehicle classification using magnetometer arrays," in *Proc. SPIE Unattended Ground, Sea, Air Sensor Technol. Appl. IV*, 2002, vol. 4743, pp. 205–212.

[6] R. J. Kozick and B. M. Sadler, "Joint processing of vector-magnetic and acoustic-sensor data," in *Proc. SPIE Unattended Ground, Sea, Air Sensor Technol. Appl. IX*, 2007, vol. 6562 [Online]. Available: http://proceedings.spiedigitallibrary.org/proceeding.aspx?articleid=1302627

[7] R. J. Kozick and B. M. Sadler, "Classification via information-theoretic fusion of vector-magnetic and acoustic sensor data," in *Proc. Int. Conf. Acoust., Speech, Signal Process.*, Apr. 2007, vol. 2, pp. II-953–II-956.

[8] R. J. Kozick and B. M. Sadler, "Algorithms for tracking with an array of magnetic sensors," in *Proc. Sensor Array Multichannel Signal Process. Workshop*, Jul. 2008, pp. 423–427.

[9] C. T. Christou and G. M. Jacyna, "Vehicle detection and localization using unattended ground magnetometer sensors," presented at the 13th Int. Conf. Inf. Fusion, Edinburgh, U.K., Jul. 2010.

[10] N. Wahlström, J. Callmer, and F. Gustafsson, "Magnetometers for tracking metallic targets," presented at the 13th Int. Conf. Inf. Fusion, Edinburgh, U.K., Jul. 2010.

[11] N. Wahlström, J. Callmer, and F. Gustafsson, "Single target tracking using vector magnetometers," in *Proc. Int. Conf. Acoust., Speech, Signal Process. (ICASSP)*, Prague, Czech Republic, May 2011, pp. 4332–4335.

[12] M. Rakijas, "Magnetic object tracking based on direct observation of magnetic sensor measurements," U.S. Patent 6 269 324, Jul. 31, 2001.

[13] L. Merlat and P. Naz, "Magnetic localization and identification of vehicles," in *Proc. SPIE Unattended Ground Sensor Technol. Appl. V*, 2003, vol. 5090, pp. 174–185.

[14] A. S. Edelstein, "Magnetic tracking methods and systems," U.S. Patent 6 675 123, Jan. 6, 2004.

[15] M. Birsan, "Non-linear Kalman filters for tracking a magnetic dipole," presented at the Int. Conf. Marine Electromagn., London, U.K., Mar. 2004.

[16] M. Birsan, "Unscented particle filter for tracking a magnetic dipole target," in *Proc. MTS/IEE OCEANS*, Washington, DC, USA, Sep. 2005.

[17] S. Y. Cheung and P. Varaiya, "Traffic surveillance by wireless sensor networks: Final report," Inst. of Transportation Studies, Univ. of California, Berkeley, CA, USA, Tech. Rep., Jan. 2007.

[18] S. Y. Cheung, S. Coleri, B. Dundar, S. Ganesh, C. W. Tan, and P. Varaiya, "Traffic measurement and vehicle classification with single magnetic sensor," *J. Transportation Res. Board*, vol. 1917, pp. 173–181, 2005 [Online]. Available: http://trb.metapress.com/content/k81k503045814723/

[19] Z. A. Daya, D. L. Hutt, and T. C. Richards, "Maritime electromagnetism and DRDC signature management research," Defence R&D Canada, Tech. Rep., Dec. 2005.

[20] M. Birsan, "Electromagnetic source localization in shallow waters using Bayesian matched-field inversion," *Inverse Problems*, vol. 22, no. 1, pp. 43–53, 2006.

[21] J. Callmer, M. Skoglund, and F. Gustafsson, "Silent localization of underwater sensors using magnetometers," *EURASIP J. Adv. Signal Process.*, 2010 [Online]. Available: http://asp.eurasipjournals.com/content/2010/1/709318

[22] J. C. Maxwell, "A dynamical theory of the electromagnetic field," *Philos. Trans. Roy. Soc. London*, vol. 155, pp. 459–513, 1865.

[23] S. M. Kay, *Fundamentals of Statistical Signal Processing: Estimation Theory*. Upper Saddle River, NJ, USA: Prentice-Hall, 1993.

[24] D. Törnqvist, "Statistical fault detection with applications to IMU disturbances," Lic. thesis, Dept. Elect. Eng., Linköping Univ., Linköping, Sweden, 2006.

[25] *"MTi and MTx User Manual and Technical Documentation,"* Xsens Technologies B.V., Enschede, The Netherlands, 2005.

[26] F. Gustafsson, *Statistical Sensor Fusion*, 1st ed. Lund, Sweden: Studentlitteratur, 2010.

Niklas Wahlström (S'11) received the M.Sc. degree in applied physics and electrical engineering in 2010 and the Tech. Lic. degree in automatic control in 2013, both from Linköping University, Sweden.

Since 2010 he is working towards the Ph.D. degree at the Division of Automatic Control, Department of Electrical Engineering, Linköping University. His research interests include sensor fusion, localization and mapping, especially using magnetic sensors.

Fredrik Gustafsson (S'91–M'93–SM'05–F'12) is professor in Sensor Informatics at Department of Electrical Engineering, Linköping University, since 2005. He received the M.Sc. degree in electrical engineering 1988 and the Ph.D. degree in automatic control, 1992, both from Linkoping University. During 1992–1999 he held various positions in automatic control, and 1999–2005 he had a professorship in Communication Systems. His research interests are in stochastic signal processing, adaptive filtering and change detection, with applications to communication, vehicular, airborne, and audio systems. He is a co-founder of the companies NIRA Dynamics (automotive safety systems), Softube (audio effects) and SenionLab (indoor positioning systems).

He was an associate editor for IEEE TRANSACTIONS OF SIGNAL PROCESSING 2000–2006 and is currently associate editor for IEEE TRANSACTIONS ON AEROSPACE AND ELECTRONIC SYSTEMS and *EURASIP Journal on Applied Signal Processing*. He was awarded the Arnberg prize by the Royal Swedish Academy of Science (KVA) 2004, elected member of the Royal Academy of Engineering Sciences (IVA) 2007, elevated to IEEE Fellow 2011 and awarded the Harry Rowe Mimno Award 2011 for the tutorial "Particle Filter Theory and Practice with Positioning Applications", which was published in the *AESS Magazine* in July 2010.